23rd ABCM International Congress of Mechanical Engineering
December 6-11, 2015, Rio de Janeiro, RJ, Brazil

ADVANCES IN THE DESIGN OF A MULTI-STAGE HYDROKINETIC TURBINE

Germán Alejandro Ibarra Bolaños
Study Group in Renewable Energies, Federal University of Itajubá, R. Dr. Pereira Cabral, 1303, Itajubá - MG, 37500-903
german.ibarra.unifei@gmail.com

Geraldo Lúcio Tiago Filho
CERPCH Executive Secretary, Federal University of Itajubá, R. Dr. Pereira Cabral, 1303, Itajubá - MG, 37500-903
tiago@unifei.edu.br

Ramiro Gustavo Ramírez Camacho
Virtual Hydrodynamics Lab., Federal University of Itajubá, R. Dr. Pereira Cabral, 1303, Itajubá - MG, 37500-903
ramirez@unifei.edu.br

Abstract. *The energy of waterways is harnessed by hydrokinetic devices, namely, turbine and oscillating systems. Current trends are focused on the use of farms and multi-rotor systems in order to increase both, efficiency and energy generation. The use of farms deals with research about arrays of modern-design systems and the interference between each other. For other hand, multi-rotor systems involve research and development of new technologies. This is the case of the multi-stage hydrokinetic turbine, a system in which several rotors are mounted on the same rotating shaft. Here, we present the results obtained so far about its performance in free-stream and confined flows. The aim is to determine the influence of each type of flow over performance, based on data obtained from computational modeling and experimental tests. Thus, wake extension and flow pattern seem to be more suitable in confined flow, where efficiency increases even exceeding the Betz limit, due to the effects of blockage area ratio. Research continues to determine the best operating conditions of the system.*

Keywords: *Hydrokinetic energy, multi-stage turbine, efficiency gain, computational fluid dynamics.*

1. INTRODUCTION

Recently, non-conventional forms of hydroelectric harnessing have experienced advances on their development. Consequently, the interest in wave, tidal and In-stream technologies is currently leading its exploration and use in different projects around the world. These projects involve a range of installed capacity (Vermaak et al. (2014)), being registered in databases that classify them depending on the technology readiness level (U.S. Department of Energy, 2014). However, to be more cost-effective hydrokinetic energy is now thought to be extracted in multi-rotor configurations like farms, as it exactly occurs in wind energy. Generally, they involve turbine arrays in parallel (one row) or staggered (various rows) (Bahaj; Myers (2013)). This is because Turnkey costs of these technologies are higher compared with other renewables for electricity generation (International Institute for Applied Systems Analysis (2012)).

Following this current tendency, we study an axial-flow hydrokinetic turbine with two rotors and the same shaft. The aim is to explore the effects of wall proximity over performance. To accomplish it, we use experimental data for confined flow condition and numerical modeling for free-stream flow. Two-rotor modeling is carried out using Computational Fluid Dynamics, based on a far-field domain. Performance and near wake characteristics are analyzed to obtain the efficiency gain produced by the use of the second rotor, even analyzing the efficiency gain derived from the angular relative position between rotors, called lag angle. At the end, the best operating conditions are discussed and some suggestions for future work are offered.

2. THE MULTI-STAGE HYDROKINETIC TURBINE

In its initial conception, this multistage hydrokinetic turbine was thought to be used in rivers. This means that any interaction with some kind of external bounding surface was not intended. The design considered some axial-flow propellers mounted on the same shaft. Thus, shaft power can be transferred to the electric generator through a coupling and a gearbox, all placed on a main structure moored or anchored to some part in the river. In theory, the water stream interacts with all rotors generating an efficiency gain. Then, part of the energy rejected by the first stage is harnessed in the second, and so on.

2.1 Model description

A model was designed, fabricated and tested at the National Center of Reference of SHP, of Federal University of Itajubá, with patent application in 2006 (BR 20 2013 006730 5). The initial attempt included 0.3m-diameter low-cost propellers to increase cost-effectiveness. Then, the system was tested in a hydraulic channel with a narrow cross section having 0.4m-width (Fig.1a), as described by Filho et al. (2010). Here, we test numerically the multi-stage turbine in its initial conception: without wall proximity. The aim is to determine how wall effects influence performance. Rotor geometry was created from dimensions of the fabricated model in CAD/CAE software (Fig.1b). After a Boolean subtraction, the Far-field fluid domain was obtained as a one-fourth of a large cylinder, with 3D of radius and 11D of length, being D the rotor diameter. In this way, working with a portion of the cylinder allowed to reduce computational cost, obtaining solutions in shorter time by means of the use of periodicity planes (Fig.1c). This is often used in literature, such as in the works of Lee et al. (2012) and Javaherchi et al. (2013).

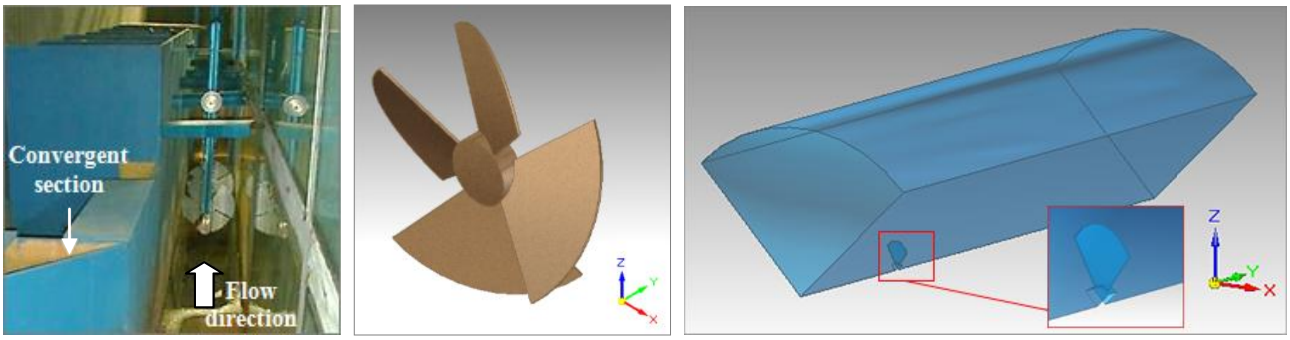

(*a*) (*b*) (*c*)

Figure 1. Multi-stage hydrokinetic turbine. (*a*) Test bench, (*b*) CAD rotor model, (*c*) Far-field geometry.

2.2 Performance assessment

Generally, performance for wind and hydrokinetic turbines is described using the following three non-dimensional coefficients: power coefficient (C_P), torque coefficient (C_Q) and the Tip Speed Ratio (λ) (Vermeer et al. (2003)):

$$C_P = \frac{T\omega}{0.5\rho A_r V^3} \tag{1}$$

$$C_Q = \frac{T}{0.5\rho R A_r V^2} \tag{2}$$

$$\lambda = \frac{\omega R}{V} \tag{3}$$

These quantities relate important variables, such as the shaft torque (T), the angular velocity (ω), the water density (ρ), the rotor swept area (A_r), the inflow velocity (V) and the rotor radius (r). Under normal operating conditions, i.e. free-stream flow, performance is influenced by rotor solidity, defined as the total rotor planform area to the total swept area. For the axial-flow rotor studied here, solidity was determined as 85.9%, therefore, it is expected a low-λ and high-torque performance, with a relative low power coefficient (Burton et al. (2011)) (Fig. 2).

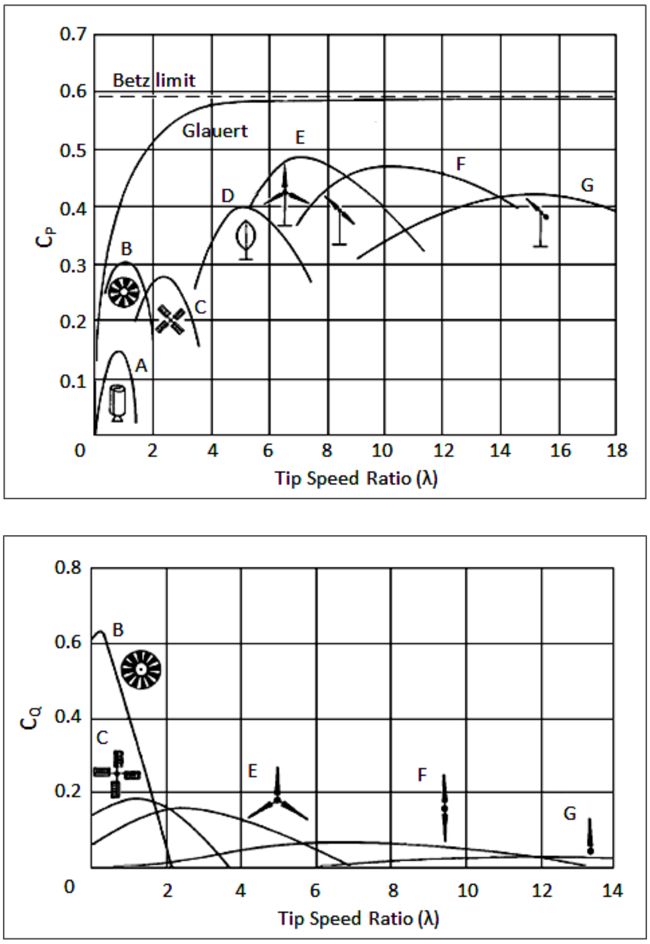

(*a*) (*b*)

Figure 2. Performance curves and solidity effects on some free-stream turbines. (*a*) Power and (*b*) torque coefficients as a function of Tip Speed Ratio (A: Savonius rotor, B: American wind turbine, C: Dutch windmill, D: Darrieus rotor, E: Three-bladed rotor, F: Two-bladed rotor, G: One-bladed rotor).

3. METHODOLOGY

For confined flow, torque, shaft rotation and flow velocity are determined experimentally using a Prony brake, a tachometer and a small current-meter, respectively. Axial separation was carried out in six different options within the range of 0.76D – 5.55D, being D rotor diameter. In addition, the relative angular position (lag angle) was varied every 10 degrees from 0 – 40 degrees. For free-stream flow, analysis is based on Computational Fluid Dynamics (CFD) using the commercial package ANSYS® FLUENT V14.0™. Flow velocity and shaft rotation are known inlet variables, in the same range of experimental campaigns: flow velocity of 1.17 – 2.0 m/s and rotation of 37 – 175 RPM. Nonetheless, torque was determined as the result of the integration of shear stresses over all blade surfaces relative to rotation axis. For the pressure-based solver, RMS residuals of the equations of mass, momentum and turbulence were found to be between $1x10^{-4}$ and $1x10^{-5}$. The SIMPLE algorithm was selected as the pressure-velocity coupling for calculating pressure field. Governing equations for conservations laws and turbulence model are presented as follows.

3.1 Governing equations

For a non-inertial rotating frame, conservation equations include some changes. First, relative component of velocity vector (***w***) replaces absolute component vector (***u***) in continuity equation. Then, it results (Ibarra et al. (2014)):

$$\frac{\partial}{\partial x_i}(\overline{\boldsymbol{w}_i}) = 0 \tag{4}$$

Here, the line over the relative velocity component represents the so called Reynolds average. Similarly, for momentum equations, non-inertial "*apparent accelerations*" ($\boldsymbol{a}_{ap}$) appear including the effects of Coriolis, centripetal and tangential components, respectively:

$$\boldsymbol{a_{ap}} = 2\boldsymbol{\omega} \times \boldsymbol{w} + \boldsymbol{\omega} \times (\boldsymbol{\omega} \times \boldsymbol{r_P}) + \boldsymbol{\omega} \times \boldsymbol{r_P} \tag{5}$$

Quantities in bold represent, in order, the vectors of angular velocity ($\boldsymbol{\omega}$), the relative velocity ($\boldsymbol{w}$) and the position of a fluid particle through the control volume ($\boldsymbol{r_P}$). Finally, momentum equation is averaged and rewritten as:

$$\rho \overline{\boldsymbol{w}}_j \frac{\partial \overline{w}_i}{\partial x_j} + \rho\left(\overline{\boldsymbol{a}}_{ap,i}\right) = -\frac{\partial \bar{p}}{\partial x_i} + \left(\mu \frac{\partial^2 \overline{w}_i}{\partial x_j^2} - \rho \frac{\partial}{\partial x_j} \overline{\boldsymbol{w}_i' \boldsymbol{w}_j'}\right) + \rho \overline{\boldsymbol{g}} \tag{6}$$

With ρ as the fluid density, μ the fluid dynamic viscosity and $\overline{\boldsymbol{g}}$ the gravitational acceleration vector. The term $-\rho \overline{\boldsymbol{w}_i' \boldsymbol{w}_j'}$ is called as the Reynolds Stress Tensor, defined as:

$$\overline{\boldsymbol{w}_i' \boldsymbol{w}_j'} = \begin{bmatrix} \overline{w_x' w_x'} & \overline{w_x' w_y'} & \overline{w_x' w_z'} \\ \overline{w_y' w_x'} & \overline{w_y' w_y'} & \overline{w_y' w_z'} \\ \overline{w_z' w_x'} & \overline{w_z' w_y'} & \overline{w_z' w_z'} \end{bmatrix} \tag{7}$$

For the $\kappa - \omega$ SST turbulence model, the Reynolds Stress Tensor is determined using Boussinesq hypothesis, based on the turbulent viscosity (μ_t):

$$-\rho \overline{\boldsymbol{w}_i' \boldsymbol{w}_j'} = \mu_t \left(\frac{\partial w_i}{\partial x_j} + \frac{\partial w_j}{\partial x_i}\right) - \frac{2}{3}\left(\rho \kappa + \mu_t \frac{w_k}{\partial x_k}\right) \delta_{ij} \tag{8}$$

Where κ is the turbulent kinetic energy and δ_{ij} is the Kronecker delta. The turbulent viscosity, a flow property, is calculated in the turbulence model. According to literature, the $\kappa - \omega$ SST turbulence model has demonstrated good results for flows with adverse pressure gradients and complex geometries (Menter et al. (2003)), such as sharp edges and corners in the rotor.

3.2 The κ-ω SST turbulence model

This model has two transport equations for the turbulent kinetic energy (κ) and the specific dissipation rate (ω). It combines the capabilities of the standard κ – ε and κ – ω models, which have good results in far and near-wall regions, respectively. The use of each model is selected automatically by the blending function (Menter (1994)). These two transport equations are defined as follows (ANSYS® (2011)):

$$\frac{\partial}{\partial t}(\rho \kappa) + \frac{\partial}{\partial x_i}(\rho \kappa u_i) = \tilde{G}_k - Y_k + \frac{\partial}{\partial x_i}\left(\Gamma_k \frac{\partial_k}{\partial x_i}\right) + S_k \tag{9}$$

$$\frac{\partial}{\partial t}(\rho \omega) + \frac{\partial}{\partial x_i}(\rho \omega u_i) = G_\omega - Y_\omega + \frac{\partial}{\partial x_j}\left(\Gamma_\omega \frac{\partial_\omega}{\partial x_j}\right) + D_\omega + S_\omega \tag{10}$$

The terms $\bar{G}_k$ and $\bar{G}_\omega$ are the production terms, Y_k and Y_ω are the dissipation terms, Γ_k and Γ_ω are the effective diffusivity terms, and S_k and S_ω are the source terms (user-defined) for κ and ω, respectively. The term D_ω is called the Cross diffusion term, which contains the mentioned blending function to change between κ – ε and κ – ω models. Another capability of the κ – ω SST model is the use of enhanced wall functions. This option helps in the modeling of the laminar sublayer and logarithmic layer within the velocity profile when a surface is present. Thus, it is not necessarily to have a so refined mesh near walls, with a suitable representation for all y^+ range (ANSYS® (2011)). In all CFD models, the maximum y^+ was 95.

3.3 Mesh and boundary conditions

Fluid domain is a far-field volume, as previously showed in Fig.1c. Rotational periodicity is set up choosing division planes of the volume. The Single Reference Frame approach is associated to all rotor surfaces, which also have the non-slip condition. The inlet has a uniform velocity profile in the axial direction (Y-axis), the same for the external surface of the cylinder; therefore, it corresponds to a translational velocity. Finally, the outlet has a zero gage pressure (Fig. 3).

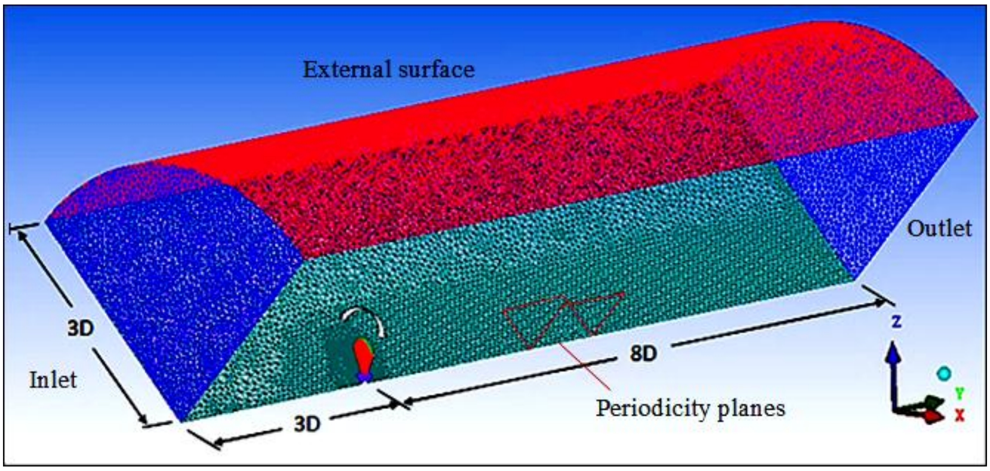

Figure 3. Far-field and boundary conditions (Rotation in *Y*-axis).

Inlet section has, also, initial defined values for the turbulent kinetic energy (κ) and the specific dissipation rate (ω), both calculated with the following expressions (Minin; Minin (2011)):

$$k = \frac{3}{2}(\bar{V}\ I)^2 \tag{11}$$

$$\omega = \frac{k^{1/2}}{C_\mu^{1/4}\ l} \tag{12}$$

The variables involved are the average velocity ($\bar{V}$), taken as the value at the inlet surface; the turbulence intensity (I), taken as 1%; one of the constants of the $\kappa - \varepsilon$ turbulence model ($C_\mu = 0.009$) and the turbulent length scale (l) based on rotor diameter D. All models are processed in a Intel® Core™ i7-3770 @ 3.4 GHz and 8GB RAM computer.

4. RESULTS

Experimental results showed that for confined flow, a single rotor produces a maximum power coefficient (C_P) of 34 per cent for a Tip Speed Ratio (λ) of 1,382 (Filho et al., 2010). The corresponding blockage area ratio, defined as rotor planform area to the flow section in the channel, was in the range of 0.34 - 0.41 per cent. It is known in literature that blockage effects, due to wall proximity, can be neglected when blockage area ratio is five per cent (Ibarra; Palacios (2013)). Then, for the flow section during tests, it can be seen that there exist blockage effects. This condition is commonly found in many laboratories due to space limitations when comparing the experimental facilities with model size (MacDonald (2012)). Therefore, some expressions are used to calculate the equivalent power coefficient in free-stream flow (Bahaj et al. 2007).

For two-rotor configuration, power coefficient has different values depending on the axial separation. The maximum value is reached for 2.43D, among all values considered in Figure 4a. For that case, lag angle variation also showed different results for the power coefficient with its maximum for zero degrees, shown in Figure 4b. Then, power coefficient varies significantly with large axial and angular positions. This suggests that near wake is different for low and high values of them, influencing a rapid recuperation of the axial velocity component.

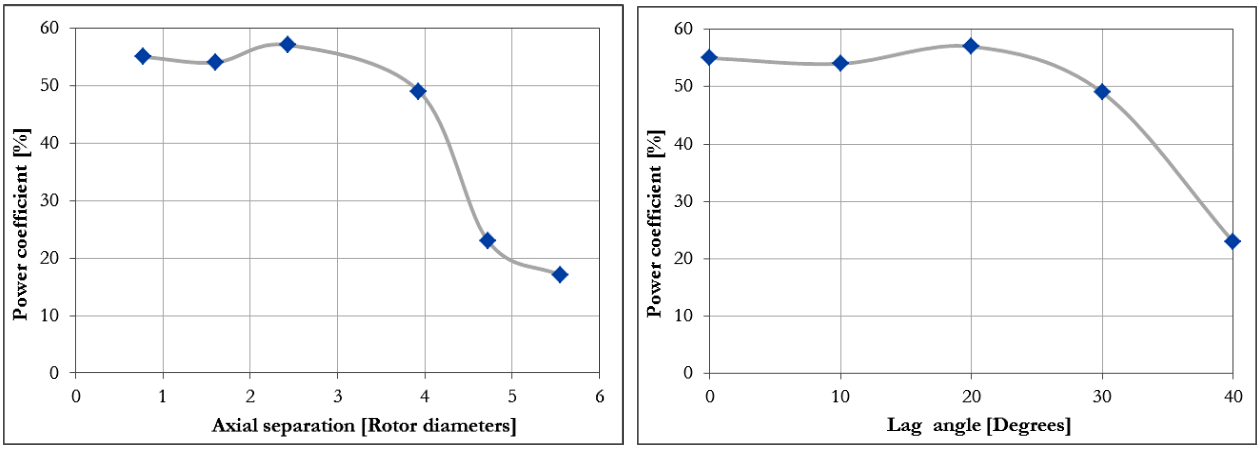

(*a*) (*b*)

Figure 4. Experimental power coefficient for a two-rotor configuration in confined flow. (*a*) Results for different axial separations, (*b*) results of angular position for 2.43D (Filho et al., 2010).

For free-stream conditions, power coefficient results for a single rotor are presented in Figure 5a. They are in concordance with general performance for high-solidity rotors, presented in Figure 2a. Maximum value corresponds to a C_P of 21.5 per cent for λ of 1,202. Considering 10 per cent as the losses in bearings and transmission components, maximum power coefficient decreases to 19.35 per cent. In fact, it can be even smaller if two important aspects are taken into account: first, the non-uniformity of velocity profiles due to the upstream convergence section (Fig. 5b) and the interference of transmission components (Fig. 5c).

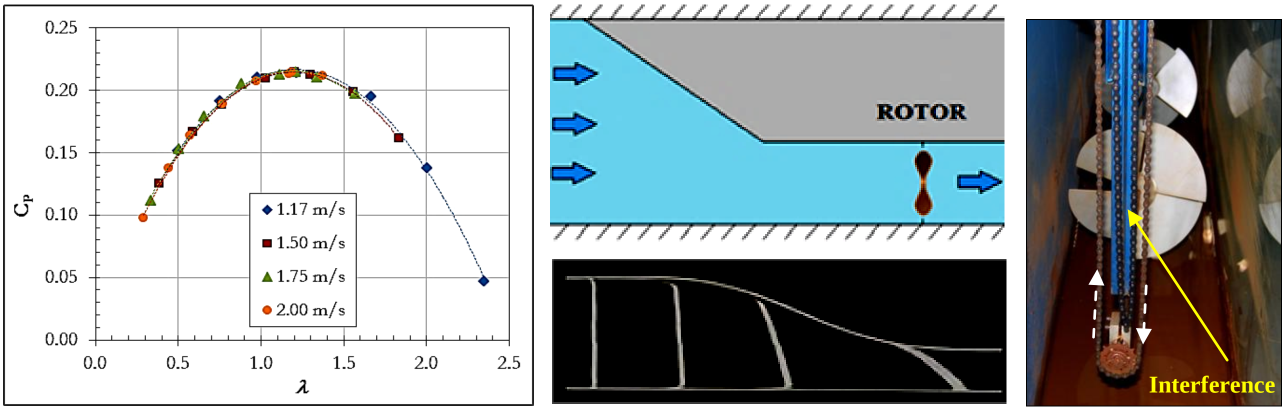

(*a*) (*b*) (*c*)

Figure 4. Aspects about results for a single rotor in free-stream flow. (*a*) Power coefficient from CFD; (*b*) non-uniform velocity profile from the asymmetric convergent section and (*c*) instabilities due to upstream transmission interference.

Consequently, it is expected an additional decrease of about 2 per cent, obtaining a power coefficient around 17 per cent. To validate this result, it is compared with the equivalent power coefficient from the experimental tests, using the expression of Bahaj et al., 2007:

$$C_{P,F} = C_{P,C}\left(\frac{V_C}{V_F}\right)^3 \tag{13}$$

Subscripts *F* and *C* refer to free-stream and confined flow, respectively. Thus, power coefficient for confined flow goes from 34 to 16.1 per cent; barely smaller than the mentioned result of 17% approximately. For other hand, Figure 5a presents the flow pattern in the near wake produced by a single rotor. This is an advantage of the use of CFD. It can be seen that there exist a core region, where the minimum velocity is located between 1-2D as mentioned by Hau (2013). Minimum axial separation for a second rotor is determined as 6D because it must be located outside the core, which is a low velocity region. This means that a freely developed wake has a larger extension in comparison to the confined flow (less than 2.43D). Placing the second rotor at 6D and varying the lag angle, the flow pattern is similar, with a gradual velocity recovery downstream (Fig. 5b).

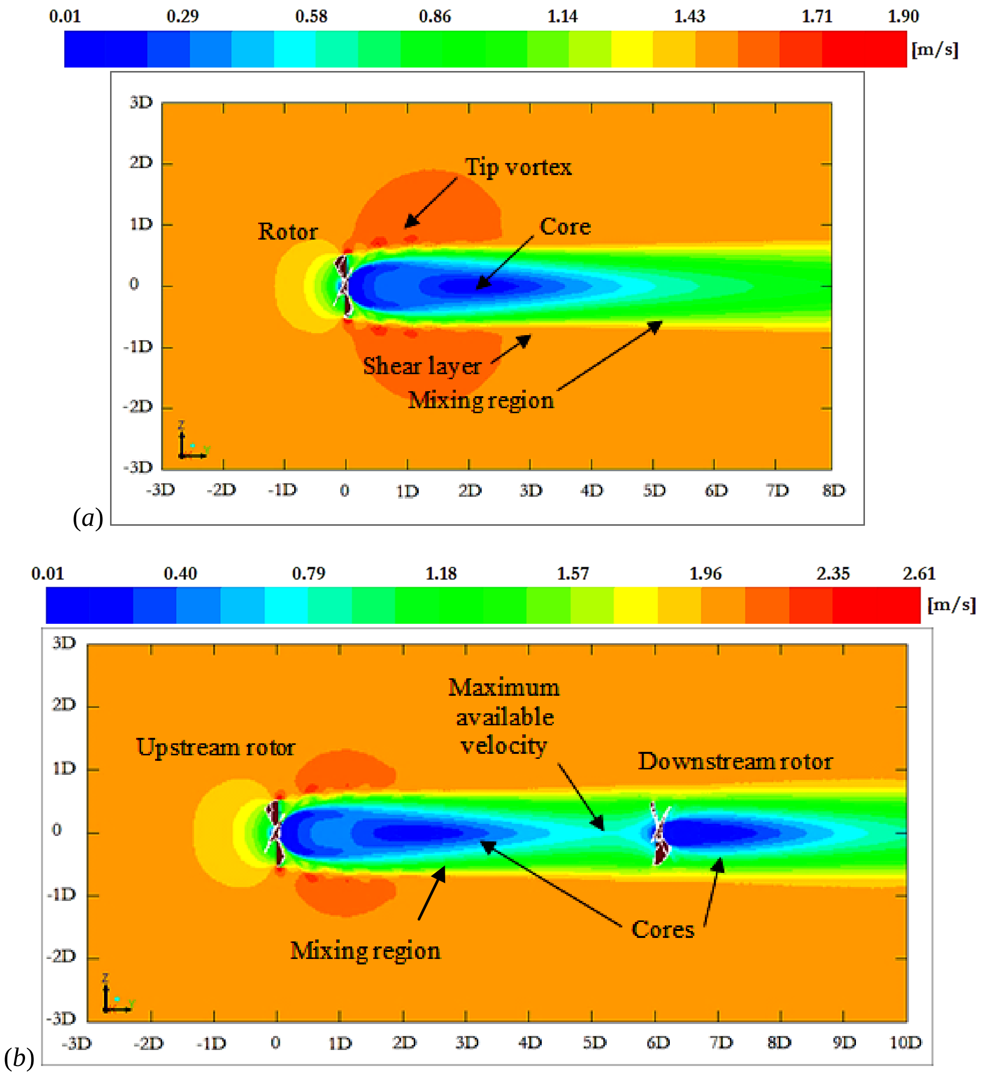

Figure 5. Flow patterns at middle plane for free-stream flow. (*a*) Results for one single rotor under a velocity of 1.5 m/s, (*b*) results for a two-rotor configuration under a velocity of 2 m/s and 67.5 degrees.

With a two-rotor configuration in free-stream flow, power coefficient is slightly larger than the one obtained for a single rotor (21.5 per cent). The difference between them is called *efficiency gain* and is showed in Figure 6 as a function of the lag angle. The gain is the range of 3.75 – 4.36 per cent and is always maximum for a lag angle of 67.5° for each velocity. This differs from the confined flow results because this efficiency gain is clearly smaller, besides it is maximum for large values of lag angle. Then, all suggest that the two flow conditions produced different results over turbine performance due to wall proximity, which helps to increase performance and shorten axial separation. Therefore, confined flow seem to be the best condition for turbine operation.

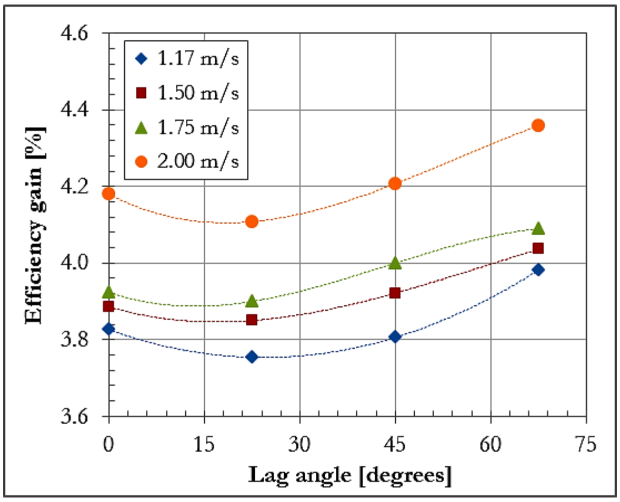

Figure 6. Results of the efficiency gain for a two-rotor configuration in free-stream flow.

5. CONCLUSIONS

In this work, the analysis of a two-rotor multistage hydrokinetic turbine under free-stream and confined flows is presented. For free-stream flow, efficiencies for one and two rotors are 21.5 and 25.9 per cent, respectively, with a maximum efficiency gain of 4.4 per cent. That gain corresponds to an axial separation of 6D and a lag angle of 67.5 degrees. The relatively low performance is the result of the rotational wake, freely developed due to the space availability. Losses are mainly caused by the high rotor solidity, which converts the most of flow energy upstream into rotational kinetic energy in both wakes.

For confined flow, efficiencies for one and two rotors are 34.0 and 57.0 per cent, respectively. In this case, efficiency gain is 23.0 per cent, exceeding the one for free-stream flow. Axial separation is just 2.43D (40.5 per cent of the free-stream flow case) for a lag angle of zero degrees. Therefore, it appears to be the best condition for turbine operation. According to literature, the influence of wall proximity (namely, blockage effects) causes a rapid recuperation of the axial component of velocity. Consequently, both rotors operate with suitable velocity diagrams because absolute velocity component is practically in the axial direction. Thus, necessarily, future developments are to be carried out based on blockage effects: within a diffuser or in a narrow hydraulic channel.

6. ACKNOWLEDGEMENTS

The authors would like to thank to the Brazilian Ministry of Mines and Energy, FAPEMIG and CAPES for funding previous and current research.

7. REFERENCES

ANSYS®. Shear-Stress Transport (SST) k- ω Model. **Academic Research Release V14.0**, 2011.

BAHAJ, A. S.; MOLLAND, A. F.; CHAPLIN, J. R.; BATTEN, W. M. J. Power and thrust measurements of marine current turbines under various hydrodynamic flow conditions in a cavitation tunnel and a towing tank. **Renewable Energy**, v. 32, n. 3, p. 407–426, 2007.

BAHAJ, A. S.; MYERS, L. E. Shaping array design of marine current energy converters through scaled experimental analysis. **Energy**, v. 59, p. 83–94, 2013. Elsevier Ltd.

BURTON, T.; SHARPE, D.; JENKINS, N.; BOSSANYI, E. **Wind Energy Handbook**. 2nd ed. John Wiley & Sons, Ltd, 2011.

FILHO, G. L. T.; SOUZA, Z. DE; ROSSI, C. A B. DE; BARROS, R. M.; SILVA, F. D. G. B. DA. “Poraque” hydrokinetic turbine. **IOP Conference Series: Earth and Environmental Science**, v. 12, p. 012094, 2010.

HAU, E. **Wind Turbines**. Third ed. Springer, 2013.

IBARRA, G. A.; PALACIOS, J. A. Criterios de diseño para un túnel de agua de bajo costo. **Ingeniería y Competitividad**, v. 15, n. 1, p. 139–149, 2013.

IBARRA, G. A.; TIAGO, G. L.; RAMIREZ, R. G. Performance and near wake analysis of a hydrokinetic rotor for multistage purposes using CFD. 10th International Conference on Hydraulic Efficiency Measurement. p.10, 2014. Itajubá, Brazil.

INTERNATIONAL INSTITUTE FOR APPLIED SYSTEMS ANALYSIS. **Global Energy Assessment**. Cambridge University Press, 2012.

JAVAHERCHI, T.; STELZENMULLER, N.; ALISEDA, A. Experimental and numerical analysis of the DOE Reference Model 1 Horizontal axis hydrokinetic turbine. Proceedings of the 1st Marine Energy Technology Symposium. p.1–10, 2013. Washington, D.C.

LEE, J. H.; PARK, S.; KIM, D. H.; RHEE, S. H.; KIM, M.-C. Computational methods for performance analysis of horizontal axis tidal stream turbines. **Applied Energy**, v. 98, p. 512–523, 2012. Elsevier Ltd.

MACDONALD, S. EquiMar Project. Disponível em: <www.equimar.org>. Acesso em: 6/1/2015.

MENTER, F. R. Two-Equation Eddy-Viscosity Turbulence Models for Engineering Applications. **AIAA Journal**, v. 32, p. 1598–1605, 1994.

MENTER, F. R.; KUNTZ, M.; LANGTRY, R. Ten Years of Industrial Experience with the SST Turbulence Model. In: K. Hanjalic; Y. Nagano; M. Tummers (Eds.); Fourth International Symposium on Turbulence, Heat and Mass Transfer. p.8, 2003. Antalya, Turkey.

MININ, I. V.; MININ, O. V. (EDS.). **Computational Fluid Dynamics Technologies and Applications**. 1st ed. InTech, 2011.

VERMAAK, H. J.; KUSAKANA, K.; KOKO, S. P. Status of micro-hydrokinetic river technology in rural applications: A review of literature. **Renewable and Sustainable Energy Reviews**, v. 29, p. 625–633, 2014. Elsevier.

VERMEER, L. J.; SØRENSEN, J. N.; CRESPO, A. Wind turbine wake aerodynamics. **Progress in Aerospace Sciences**, v. 39, n. 6-7, p. 467–510, 2003.

8. RESPONSIBILITY NOTICE

The authors are the only responsible for the printed material included in this paper.